Advanced comparison of CFD Fluent code with experimental data on a transverse flow across rod bundle using LDV, PIV, Optical Flow and POD

J. WILLIAM[a,(1)], V. FICHET[b,(2)], N. GOREAUD[c,(2)]

a. AREVA NP SAS – Montigny-Le-Bretonneux - France - johann.william@areva.com
b. AREVA NP SAS– Centre Technique Le Creusot - France – vincent.fichet@areva.com
c. AREVA NP SAS – Lyon - France – nicolas.goreaud@areva.com

Abstract

This paper presents the capability of the Computational Fluid Dynamics (CFD) Fluent V15.0 software to predict the transverse single phase flow across a rod bundle using Large Eddy Simulation (LES). To meet this objective, an advanced comparison with non-intrusive velocity measurements (Laser Doppler Velocimetry /LDV/, Particle Image Velocimetry based on cross-correlation /PIV/ and based on Optical Flow /OF/) is carried out. Beyond the classical comparison of time-averaged (mean) and standard deviation velocity profiles (spatial information), the turbulent flow is analyzed via local Power Spectral Densities /PSD/ and Proper Orthogonal Decomposition /POD/ comparison. Generally applied to academic cases (e.g. flow past a cylinder at Re = 100), POD is conducted in this paper on both CFD and PIV turbulent velocity fields around a rod inside a rod bundle. Through the spectral and fluctuating energy content of a turbulent flow, the Fluent LES turbulent model is further validated on a complex industrial test case (rod bundle mock-up of a water pressurized steam generator).

Key words: LES / PIV / LDV / Optical Flow / POD / tube or rod bundle

1. Introduction

Flow induced vibration is a generic problem that nuclear engineering tries to prevent in order to limit the equipment wear. Among equipment that may be concerned by this phenomenon is the Steam Generator (SG). When entering in liquid phase in this boiling heat exchanger, the water of the secondary loop induces a transverse flow that contributes to the tube bundle vibration. The knowledge of velocity field across the rod bundle is accordingly of importance. Investigation on flow induced vibration in transverse cross-flows can be made experimentally on a specific geometry (tube diameter/thickness/length or pitch) and on a limited number of measurements, or through the use of adequate engineering methods. In the last past years, it has been also judged interesting to access to more information using CFD simulation once CFD software and models are validated on experimental points, as these detailed simulations can help reducing excessive margins and in a general manner improve physical understanding

(1) Now at NEW AREVA – AP/DTI

(2) Now at NEW AREVA NP - DTI

and hence, design. As a consequence, AREVA launched an experimental and computational program to study single phase transverse cross-flow in rod bundle configuration close to the geometry encountered at the entrance of the downcomer of a SG. The turbulent flow inside the rod bundle is analyzed via non-intrusive velocity measurements and LES calculations. With reliable experimental data, classical comparisons of time averaged velocity and standard deviation 2D fields and profiles are undertaken. However, in order to further validate the CFD model, a numerical / experimental comparison of PSD (spectral information) is provided on one probe and the results of POD analysis on both PIV and CFD velocity fields are compared.

2. Experimental approach

2.1. Mock-up description

The experimental mock-up is composed of an upstream bent circular pipe, a flexible junction (called “dilatoflex”), an inlet divergent, a rectangular test section made of Plexiglas where the rod bundle is settled and an outlet convergent. The rod bundle consists of 5 rows of 7 rods arranged in square pitch and located at a 158 mm distance from the divergent outlet.
The characteristic dimensions of the mock-up test section are the following:

- Rod diameter : 19.05 mm equal to the SG tube outer diameter;
- Square pitch : 27.43 mm equal to the SG square pitch value;
- Straight length (between divergent outlet and convergent inlet): 500 mm;
- Height of the rods : 145 mm;

The experimental setup containing the rod bundle mock-up is illustrated in Figure 1.

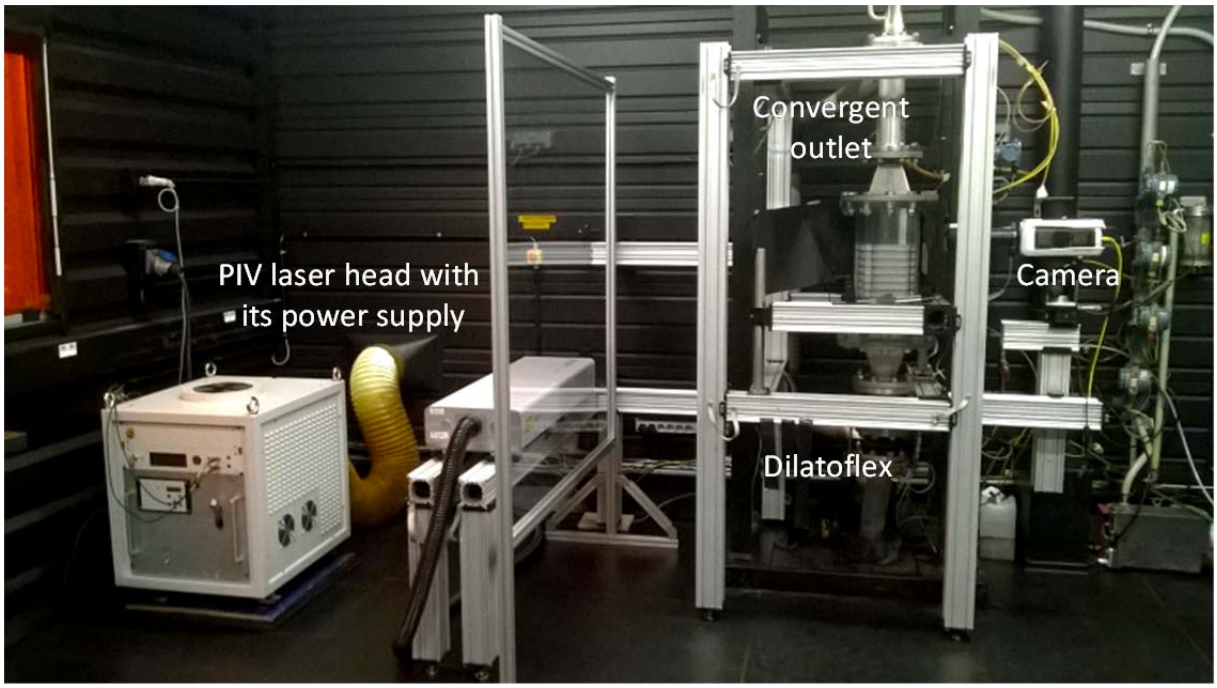

Figure 1 : Experimental setup (rod bundle mock-up, laser and camera for PIV measurements)

2.2. Velocity measuring techniques

Two non-intrusive velocity measuring techniques have been deployed to get either local components of velocity by LDV or high-speed 2D velocity fields around a rod in the mid-depth plane (half of the rod elevation normal to the rod axis) of the central row by PIV.

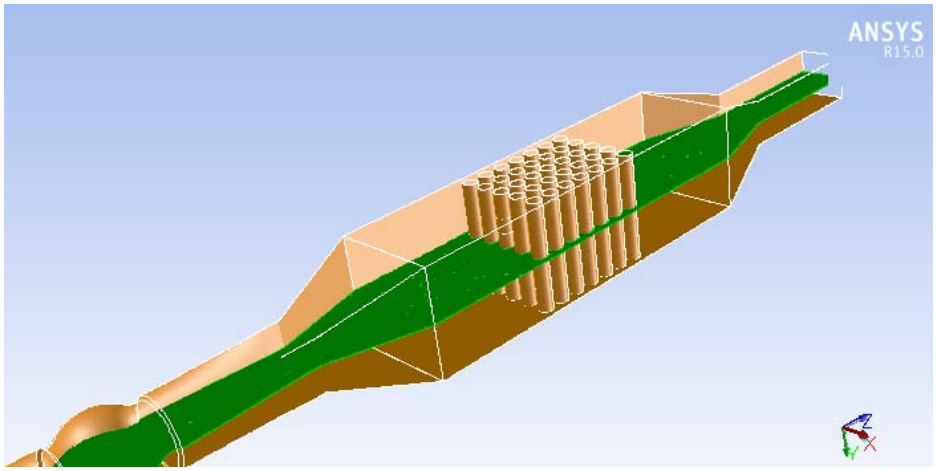

Figure 2: View of the mid-depth plane (green) located at half of the rod height

2.2.1. Index matching technique

An index matching technique is used to realize non-intrusive velocity measurements inside the rod bundle. The refractive index of 1.49 for the solid parts made of Plexiglas (rods) is matched with the fluid one, as the fluid is a mix of water and sodium iodide at the concentration required to reach the same value at 25°C (fluid density of 1.8).

2.2.2. Seeding particles

For both LDV and PIV measurements, the turbulent flow is seeded with S-HGS particles (Silver coated – Hollow Glass Spheres) manufactured by DANTEC. These particles (mean diameter of 10 µm, density of 1.5) could be considered as perfect fluid tracers up to 2 kHz.

2.2.3. Laser Doppler Velocimetry

Laser Doppler Velocimetry (LDV) has been used for 50 years [1] and has become nowadays a reference measuring tool commonly deployed in research centres to acquire fast fluctuating flow velocities in one point (local measurement).

For the present study, LDV measurements have been realized with a DANTEC FlowExplorer (wavelength 532 nm) placed on a 3 axes Charlyrobot moving support (precision ± 0.5 mm) remotely controlled by an ISEL C142-1 device. A 200 mm focal lens is set on the laser head and produces an ellipsoidal measuring volume of a 0.052 mm diameter and 0.351 mm length in air. Velocities are obtained with dedicated BSA Flow 5.10 software.

The 3 velocity components are measured on 4 probes located upstream (down), downstream (top), on the left and on the right of the 6th central rod (second to last central rod counting from upstream to downstream) in mid-depth plane. The LDV probes are precisely placed at mid-distance to the neighbouring rods (around 13.7 mm from the rod centre). Acquisition duration was over 120 seconds or once 50 000 velocities are acquired. This allows getting converged statistics (mean, standard deviation and distribution) for every velocity component. LDV acquired samples are randomly distributed in time since each sample corresponds to a particle crossing the ellipsoidal measuring volume. To plot Power Spectral Densities (PSD) using classical Fast Fourier Transform (FFT) algorithms, a time resampling of LDV samples at constant frequency (2 kHz in the present study) is carried out with a dedicated algorithm based on the time signal reconstruction proposed by Veynante and Candel ([2] and [3]).

2.2.4. Particle Image Velocimetry

Even if PIV has been developed many years after LDV [4], the interest of the scientific community for this technique has multiplied the research studies [5] aiming at improving its performance and accessibility during the last twenty years [6].

For the present study, PIV measurements have been realized with a Double cavity YLF Litron Laser (repetition rate up to 10 kHz) and a Phantom V611 camera (repetition rate up to 6 kHz in full resolution of 1280 x 800 pixels²) associated with a Nikon AF DC-Nikkor (105 mm focal length, f/2.8 aperture) The laser beam is conveyed to the test-section by a set of mirrors and converted into sheet by a series of optical lenses. Both laser sheet and camera are moved and aligned with micrometric motorized Zaber linear systems.

PIV measurements have been also performed around the 6th central rod in the mid-depth in order to be compared with LDV measurements.

A raw PIV image around the 6th central rod as well as the location of LDV measurements are given in Figure 3.

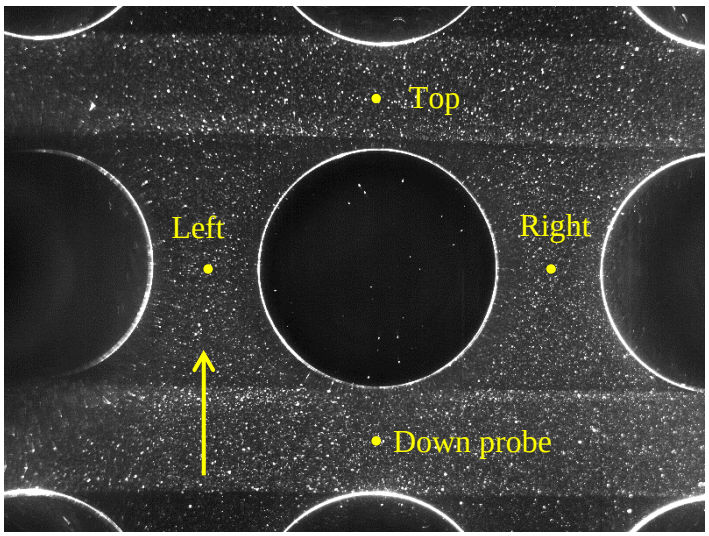

Figure 3: Raw PIV image around the 6th central rod (in the mid-depth plane) – location of LDV measurements (yellow points)

Particle image pairs are separated by a time step of 100 µs and acquired at a repetition rate of 2 kHz. The acquisition was restricted to 10 000 image pairs due to the limited storage capacity of the high speed Phantom camera (thus yielding 5 seconds of physical time acquisition). PIV image pairs are post-processed with Matlab via a parallelized version of PIVlab 1.4. This allows getting a sufficiently converged 2D mean velocity and standard deviation velocity fields in the mi-depth plane around the 6th central rod.

2.2.5. Optical Flow

Initially developed in the vision and pattern recognition domain [7], the optical flow (OF) is applied in the present paper on PIV images instead of the cross-correlation as image post-processing to get the velocity field. Based on the same PIV images, OF provides much higher spatial resolution for the velocity field (i.e. one velocity vector per pixel) than those issued from PIV based on cross-correlation (e.g. one velocity vector per 8x8 pixels² window size).
The principle of this image post-processing is to solve a convectional transport equation for the image luminosity φ (shades of grey for 8 bits images in the present study) written as:

$$\frac{\partial \varphi}{\partial t} + u\frac{\partial \varphi}{\partial x} + v\frac{\partial \varphi}{\partial y} = 0$$

The time derivative of the scalar variable φ is given by the difference of luminosity pixel by pixel between two images separated by a time step. u and v are the displacement components in the plane of the laser sheet and constitute the unknowns to be solved. Associated with the camera settings (magnification in “meter/pixel”) and the time step, they lead to high resolution velocity fields (e.g. 64 times higher than those produced by cross-correlation). A dedicated script of optical flow for PIV has been written and used with MATLAB 2016a.

OF allows getting a finer description of velocity, especially near the rod, and has been applied on PIV image pairs around the 6th central rod in the mid-depth plane.

2.3. Experimental results

In order to provide reliable data for CFD turbulent model validation, a spatial comparison of PIV (based on cross-correlation) and OF image post-processing is carried out. LDV measurements are considered as reference to validate locally the 2D velocity fields.

The PIV and OF horizontal profiles (crossing the rod centre) of mean velocity norm are compared to each other and to the LDV axial velocity at left and right probes location in Figure 4. The same comparison on standard deviation on velocity norm is displayed on Figure 5.

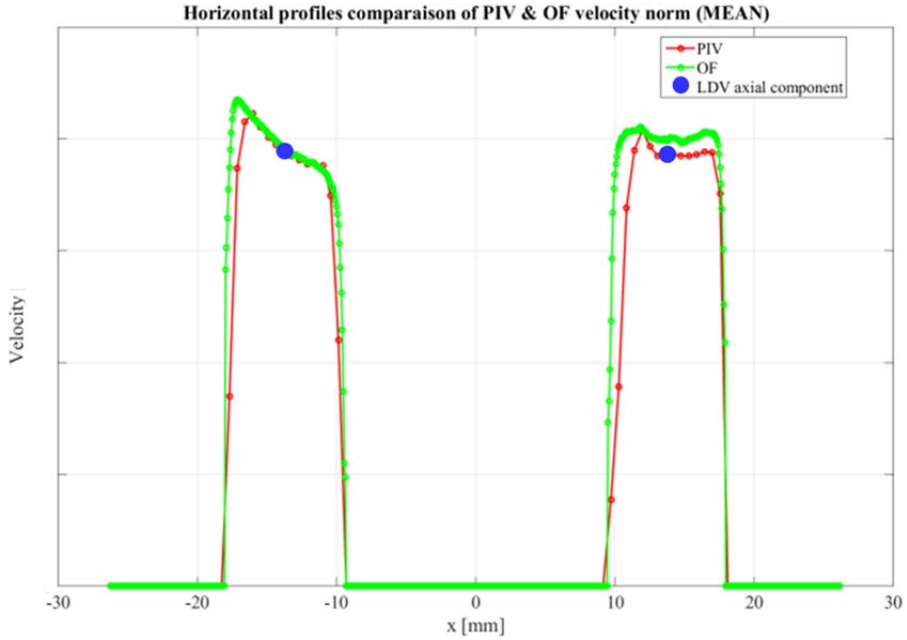

Figure 4: Horizontal profiles of mean 2D velocity norm in PIV & OF with LDV axial velocity given as reference for validation

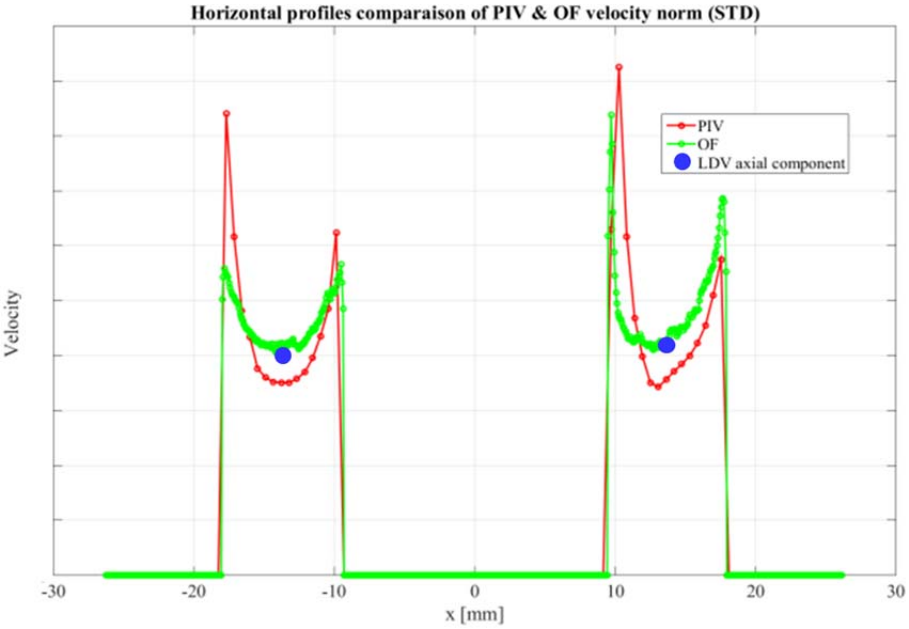

Figure 5: Horizontal profiles of standard deviation 2D velocity norm in PIV & OF with LDV axial velocity given as reference for validation.

PIV and OF results are in good agreement in terms of spatial distributions and amplitudes (same scales are used). The PIV and OF velocity norm equals the LDV axial velocity at the left and right LDV probes meaning that the transverse velocity contribution is almost null at these probes and that the PIV / OF results provide reliable data for CFD validation. It has to be noted that the mean velocity profile is quite flat on the right side (except in the boundary layer), whereas a peak of velocity is visible on the left side of the left jet.

One can also point out that OF captures much better the velocity decrease near the rod walls due to its higher spatial resolution. This is underlined by the fields of the velocity norm standard deviation issued from PIV and OF in the mid-depth plane around the 6th central rod presented in Figure 6 (same scales are used).

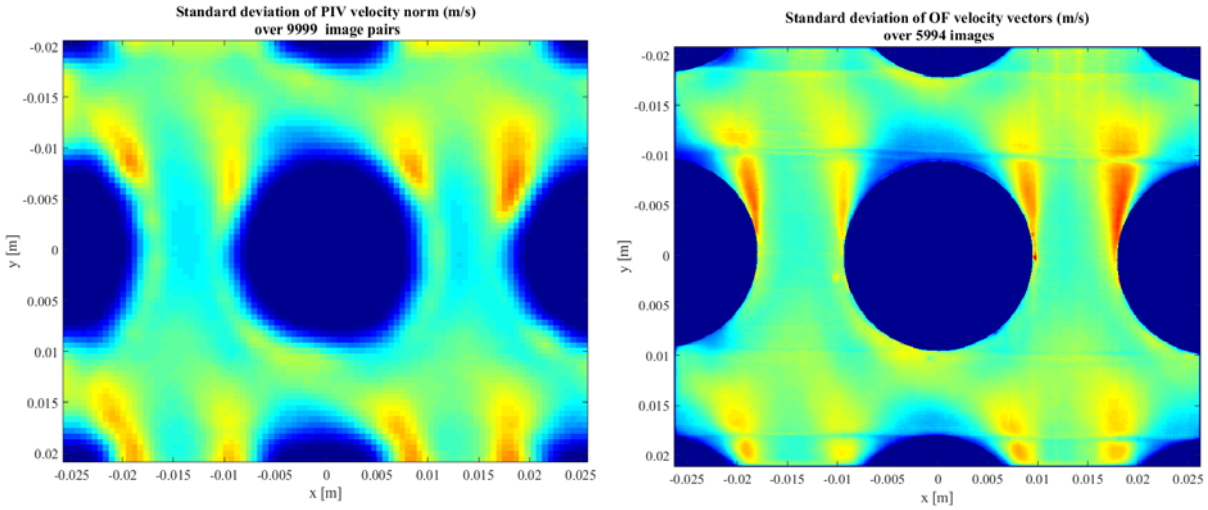

Figure 6: Standard deviation (time averaged) fields of 2D velocity norm in PIV (left) and OF (right)

It must be noticed that OF calculations have been restricted to 5994 image pairs for numerical reasons (memory limitation although a 192 Go RAM dedicated workstation has been used). The separation point (on the rod surface) and high fluctuation zones are better captured by OF. One may also observe noisy horizontal lines on the OF field. These are caused by a shadowing effect of transparent rod periphery as the laser sheet is coming from the right of the image (see Figure 3). The subsequent gradient in light intensity is taken into account by OF calculations and impacts the results.

3. Numerical approach

The CFD model is developed with the ANSYS FLUENT V15.0. This software is able to solve the Navier-Stokes equations system on a complex mesh, in transient, and includes various turbulent models.

3.1. Geometry & Mesh

The geometry represents the mock-up and around 2 meters of upstream line so as to be the most representative of the flow distribution at the rod bundle mock-up entrance. The mesh of the global domain is composed of around 90 million fluid cells (distributed between tetrahedral and hexahedral/pentas). The boundary layer is composed of 8 layers and the size of the first layer is chosen so as to respect a y^+ lower than 1.

A view of the mesh around the 6th central rod is displayed on Figure 7 and Figure 8.

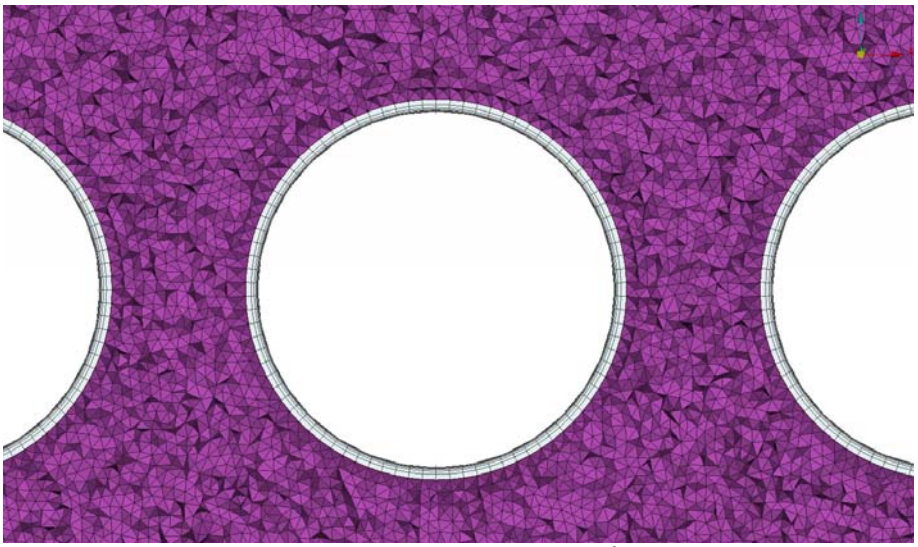

Figure 7: View of the mesh around the 6th central rod

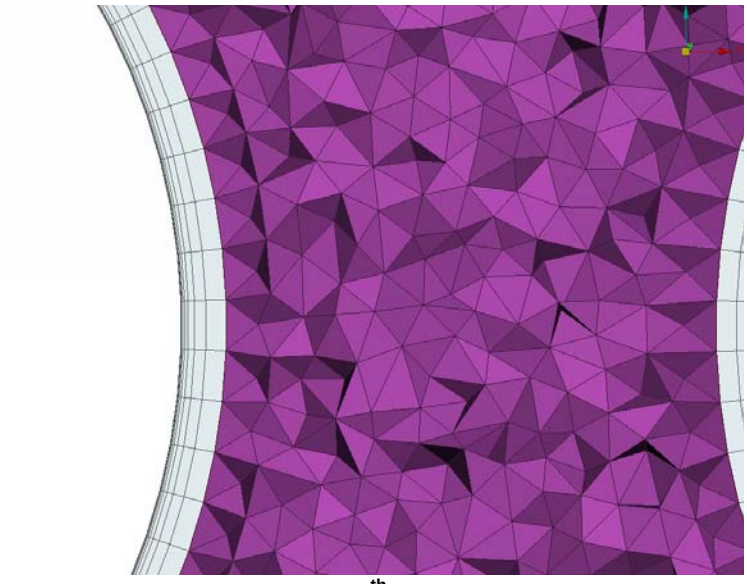

Figure 8: Close-up of the mesh around the 6th central rod - 8 layers in the boundary layer

3.2. Turbulence modelling

State of the art on unsteady flow/structure interactions modelling often refers to study of a transverse uniform flow in an infinite medium across a single tube at low Reynolds number. Modelling teams tend to reproduce PIV or hotwire velocity profiles measurements in the wake of the cylinder using Direct Numerical Simulation (DNS) or Large Eddy Simulation (LES) turbulence models [8]. For DNS, none flow modelling is required except the fluid behaviour law. The consequence is that an extremely fine mesh is required so as to solve all the spatial scales of the turbulence up-to the smallest dissipative scales in the Kolmogorov micro-scales. LES approach is a “mix” between URANS approach (Unsteady Reynolds Averaged Navier-Stokes) and DNS where large turbulence scales (carrying energy) are solved and small scales are modelled thanks to a low-pass filtering of Navier-Stokes equations.

In the frame of the present study with an industrial rod bundle configuration, a DNS approach was unfeasible, so an LES model with the Smagorinsky-Lilly (SL) turbulent sub-model was used to keep a fine representation of the flow. This choice is justified regarding reference [9] in which the authors compare the normalized velocities obtained by PIV for a flow between 2 consecutive cylinders with those obtained with various turbulent LES models: better results were observed in the wake of the first cylinder with the SL sub-model (compared to the Wall Adapting Eddy Viscosity – WALE - sub-model). It has to be noted that in reference [9], the authors mention that WALE model gives better predictions on the variation of coefficient of pressure profile for the front cylinder than SL model. Our objective in the present work was to capture the velocity field between rods as fine as possible, so the SL model has been retained in first approach based on this consideration. A sensitivity study to WALE sub-model should be carried out so as to confirm the observation made in reference [10] in which the WALE model perform slightly better than Smagorinsky model and to evaluate the impact on POD analysis since the WALE model is able to calculate the true velocity gradient tensor. Concerning the initialization of turbulence at the domain inlet, the vortexes method, settled to 190, is retained (default value in FLUENT).

3.3. Methodology

A first computation is carried out in RANS steady-state with the k-ω-SST turbulent model in order to establish a velocity field used as initial condition for the LES turbulent model transient computation. The 1.5 first seconds of the transient computation used to establish transient turbulent flow and velocity fields have not been recorded. The 3.1 next seconds have been used to constitute the data base for the POD analysis and for comparison with 2D plane PIV or OF velocity measurements. Concerning numerical parameters, a time-step of 0.5 ms with 15 sub-iterations per time-step has been retained. An example of statistical evolution of velocity probes around the 6th rod (left and top) and their standard deviation used to follow the temporal convergence are shown on Figure 9 and Figure 10.

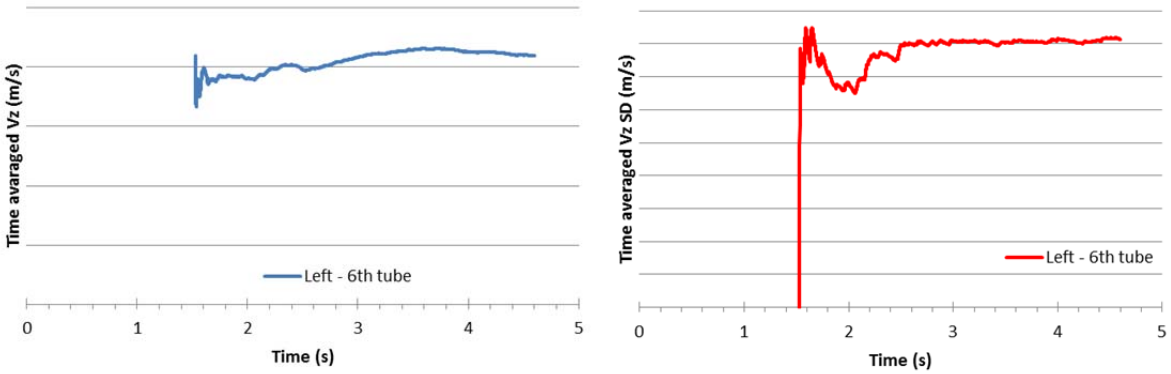

Figure 9: time history on Vz velocity (left picture) and its standard deviation (right picture) on left probe

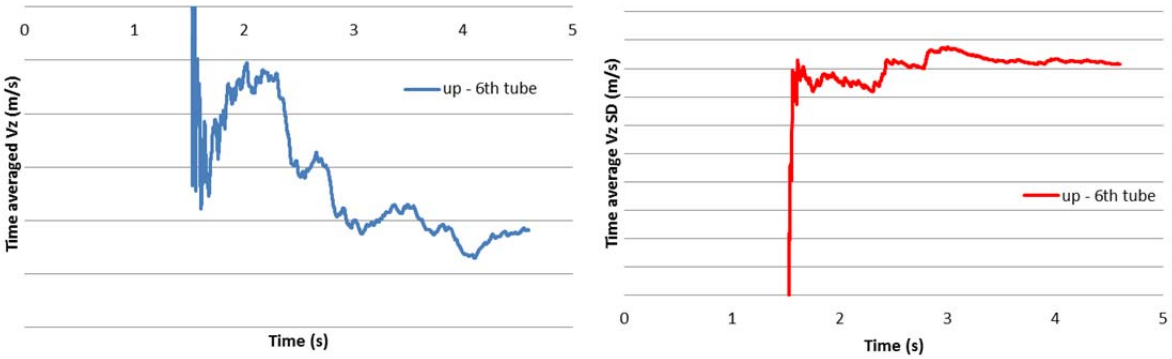

Figure 10: time history on Vz velocity (left picture) and its standard deviation (right picture) on top probe

4. Results & Discussion

4.1. Spatial validation of CFD results

To confirm that LES computation predicts correctly the flow structure in the rod bundle, LES and OF mean velocity fields around the 6th rod are compared in Figure 11.

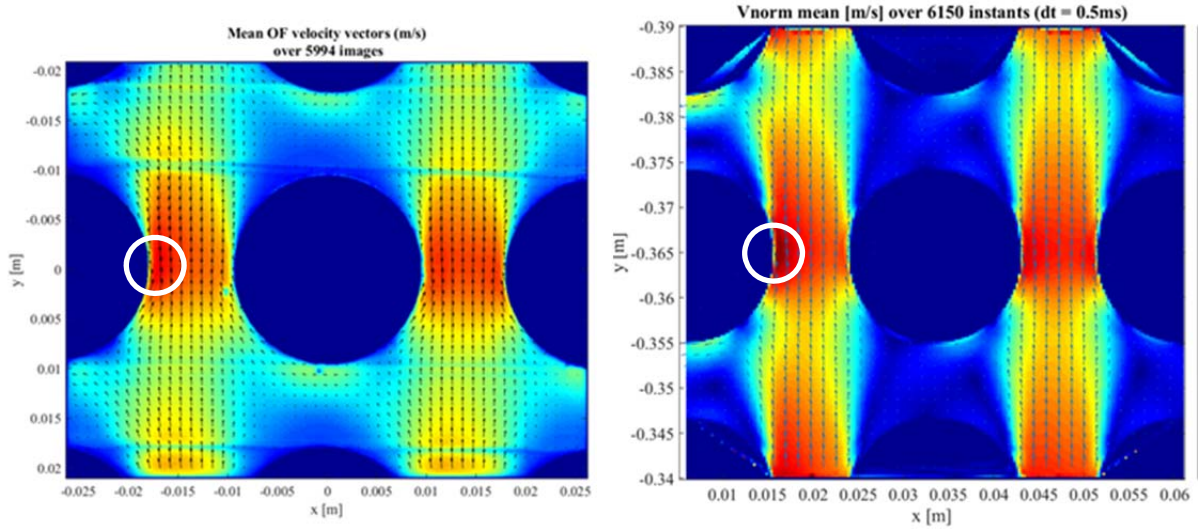

Figure 11: Comparison of mean velocity (norm) between OF (on the left) and CFD-LES (on the right) – same velocity scale

Beyond a globally good agreement between LES and OF results in terms of spatial structure, velocity vector orientation and amplitude, it can be seen that CFD predicts an asymmetrical jet on the left side of the 6th central one (as illustrated by white circles in Figure 11) with a peak of velocity on the left side of the jet (as the one observed on the velocity profiles in Figure 4).

In order to strengthen the experiment/CFD-LES comparison, velocity profiles (time averaged and standard deviation - SD) along a horizontal line crossing the 6th rod centre, left and right probes, are plotted on Figure 12.

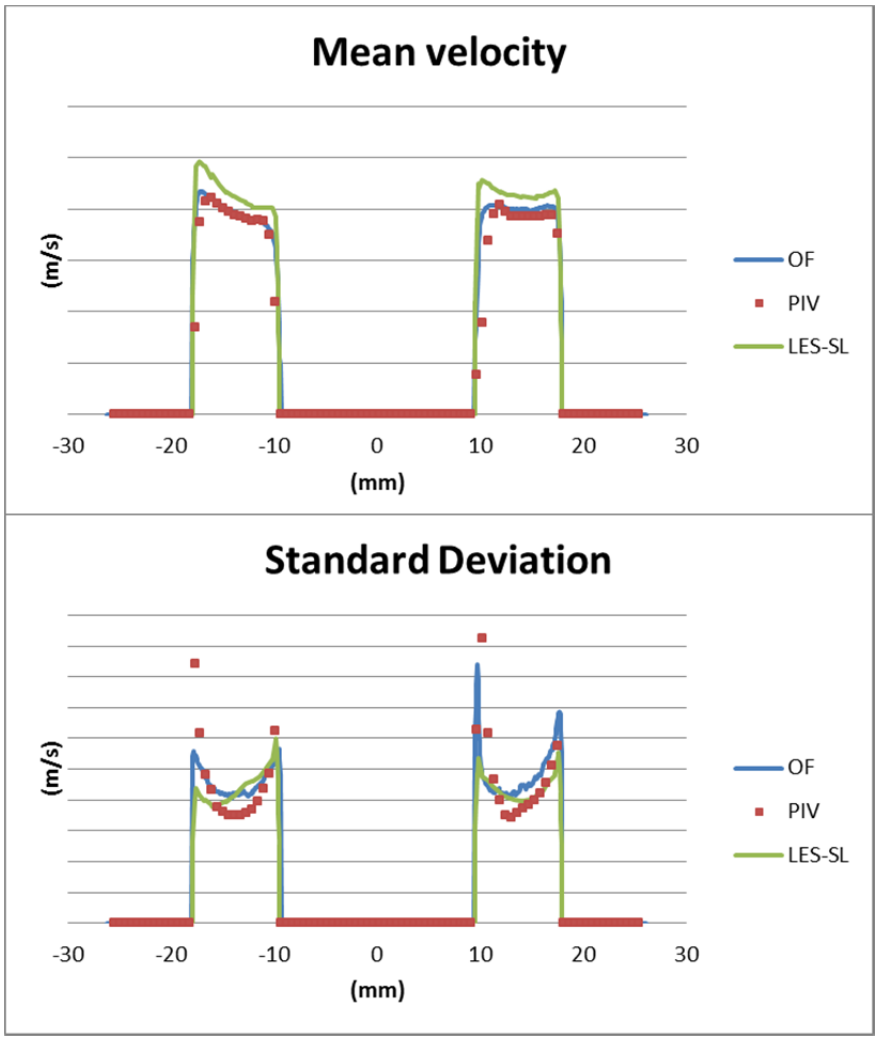

Figure 12: Comparison of mean velocity (up) and SD (down) between OF/PIV and CFD-LES –line crossing left/right probes on the 6th rod

Velocity profiles (time averaged and standard deviation) along a vertical line crossing the 6th rod centre, down and top probes are plotted on Figure 13.

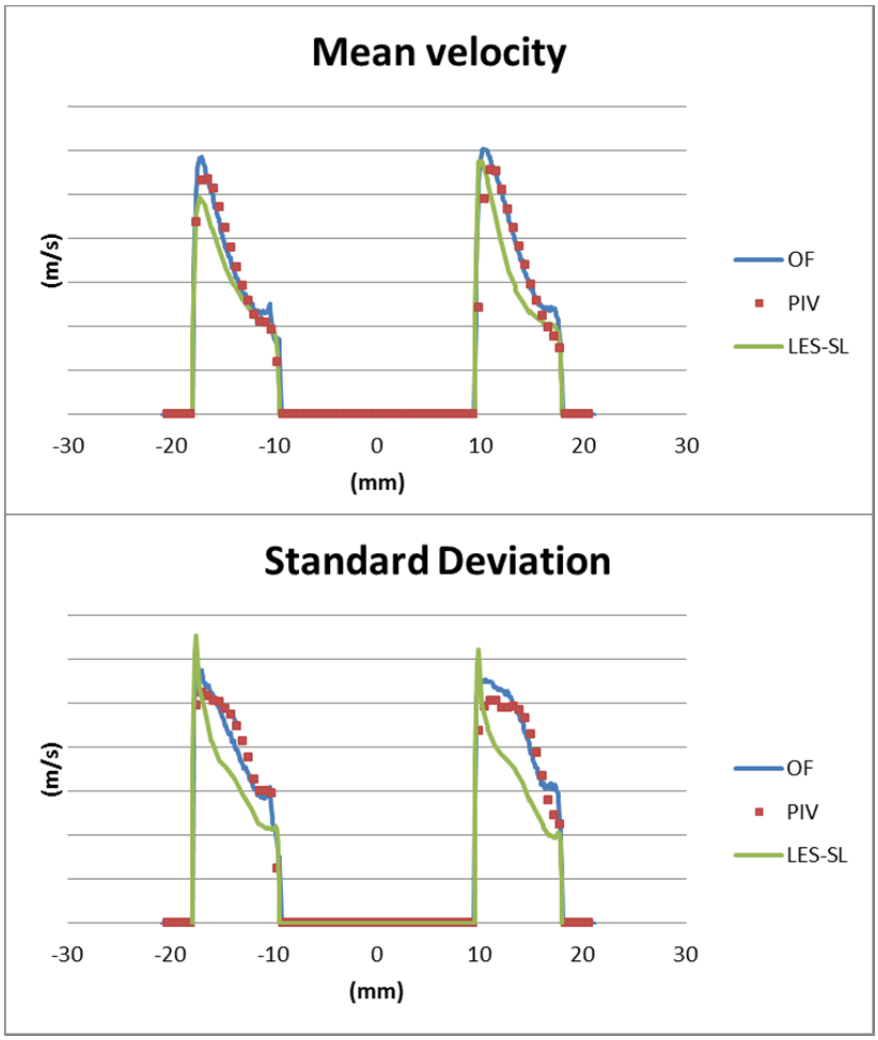

Figure 13: Comparison of mean velocity (up) and SD (down) between OF/PIV and CFD-LES –line crossing top/down probes on the 6th rod

Time averaged (mean) LES velocity profiles present very satisfactory results compared to experimental data, even if a slight over-velocity is observed along the horizontal line (crossing left/right probes).

Concerning the velocity SD profiles in Figure 13, LES results are in good agreement with experiments in terms of shapes and amplitudes even if some discrepancies are observed along the vertical line (crossing top/down probes). LES-Smagorinsky-Lilly model tends to underestimate the velocity fluctuations, probably because of a weakness to predict the pressure coefficient distribution around a cylinder (and thus, the separation point in the boundary layer). The WALE model may lead to a better prediction on this point.

Regarding these results, it can reasonably be considered that transient LES-Smagorinsky-Lilly sub-model computation with FLUENT code is validated with the settings and mesh used.

4.2. Spectral validation of CFD results

To reinforce the CFD results validation, a comparison of Power Spectral Densities (PSD) between LES and all measuring techniques is conducted (see Figure 14) at the left probe to assess the capacity of Fluent in capturing the flow behaviour in the spectral domain.

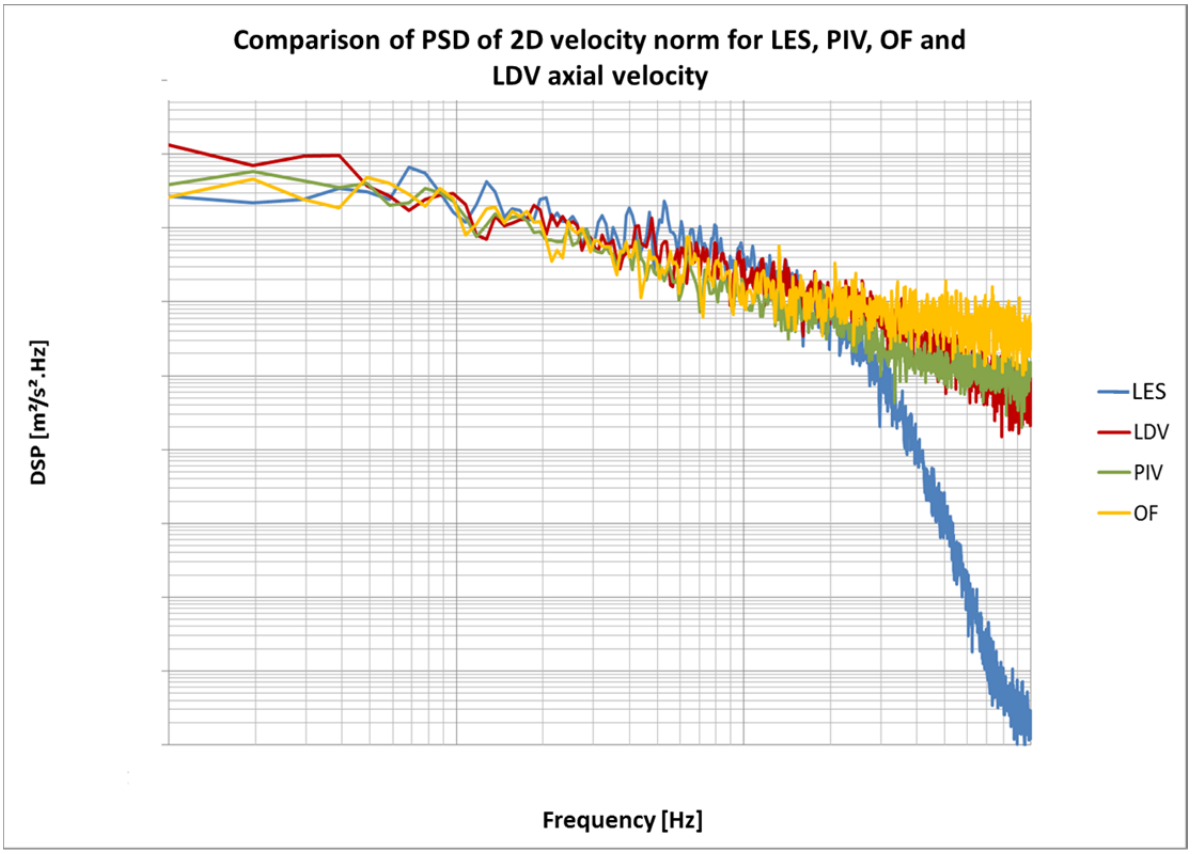

Figure 14: Comparison of PSD of velocity norm for LES, PIV, OF and LDV axial velocity at the left probe

It must be noticed that this Power Spectral Density (PSD) comparison has been made on 3 seconds time samples to match the restricted time length of LES (as well as PIV and OF) extracted signals in contrast with the 120 seconds of LDV acquisitions. PSD have been obtained over 1024 spectral points (Hanning window, window overlap of 75%).

LES predictions match well experimental results in the lower and medium frequencies (first $4/5^{th}$ of the frequency range). Beyond (last $1/5^{th}$ of the frequency range), the LES spectrum collapses. Regarding the industrial application, the LES predictions over the first $4/5^{th}$ of the frequency range are sufficient to cover the frequency range of interest for SG rod bundle excitation. One explanation of this LES spectrum collapsing is probably linked to the different characteristic mesh size used in the whole domain that could filter high frequency vortices and also due to the over-dissipation of the model. On the other hand, experimental PSD do not collapse at high frequencies, probably due to the fact that the noise, included in all measurements, contributes to PSD level at lower spatial scales (high frequencies).

The PSD of OF is more subject to that experimental noise since OF has been applied on raw images without any image pre-processing.

The same phenomenon is observed over the different probes when compared to the full length LDV signals only as shown in Figure 15.

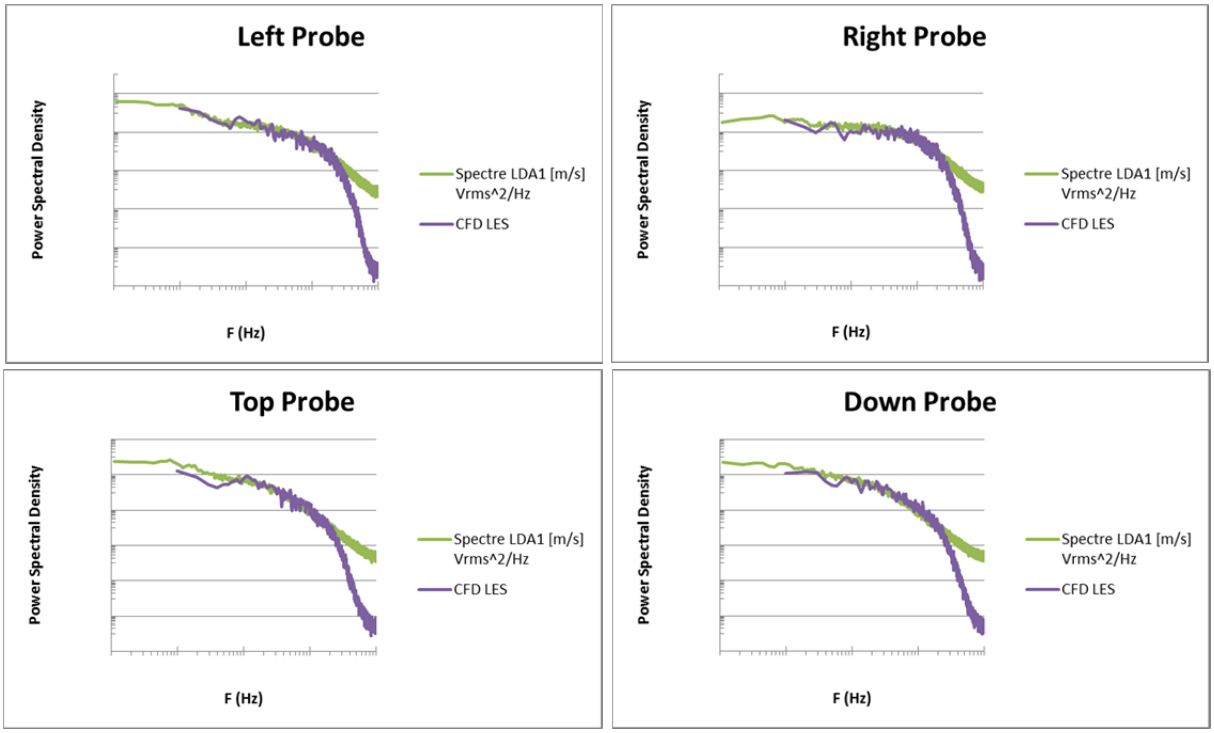

Figure 15: Comparison of PSD on axial velocity between LDV and CFD-LES – 4 probe positions – 6th rod

PSD of LDV and LES fit well together over to the first 4/5th of the frequency range. This validates the capacity of Fluent in capturing the flow behavior in the spectral domain.

4.3. CFD results validation via POD analysis

In order to achieve the advanced comparison of CFD results with experimental data proposed in this paper, a POD analysis is realized on both 2D velocity fields issued from LES and PIV around the 6th central rod. It was indeed not feasible to apply POD analysis on OF experimental results for numerical reasons (memory limitation).

4.3.1. POD description

Originally described 35 years ago [11], the Proper Orthogonal Decomposition (POD) allows extracting coherent structures from a turbulent flow. This decomposition calculates time and memory consuming spatial correlations to solve an eigen-value problem. A 'POD snapshots' method [12] has been developed to reduce the numerical burden, replacing spatial correlations by time correlations in a mathematically equivalent expression of the eigen-value problem.
In the present study, the POD snapshot method is applied on sets of instantaneous (fluctuating part only after retrieving the mean value) 2D velocity fields $\vec{v}\,(\vec{x},t)$ which are decomposed onto orthogonal bases defined as followed:

$$\vec{v}\,(\vec{x},t) = \sum_{k=1}^{\infty} A_k(t)\vec{\phi}_k(\vec{x})$$

where k represents the mode number, $\vec{\phi}_k(\vec{x})$ the eigenvector associated to the kth mode in the orthogonal base and $A_k(t)$ the time coefficient of the kth mode associated to the eigenvector.

The orthogonal base retained for the decomposition is optimal from an energetic perspective. The generated POD modes are thus sorted in a descending order of fluctuating energy.

This POD snapshot method allows:

- identifying the coherent structures of a fluctuating signal;
- getting a representation of the energy distribution;
- reconstructing the velocity field using a low number of modes while losing little information (as function of the truncation order chosen).

POD constitutes indeed a base for reduced order models where a limited number of modes (the most energetic ones) is sufficient to represent the main characteristics of a flow (e.g. flow past a cylinder at Re = 100). If 90% of the fluctuating energy is included in less than 30 modes, it could be considered fruitful to generate a reduced order model from POD for further investigations.

4.3.2. Comparison of POD results between PIV and LES

The same sample lengths between LES and PIV have been considered (6150 time samples) for POD analysis making the POD analysis comparable from a statistical perspective.
At first, the cumulated fluctuating energy is plotted as function of mode number in Figure 16.

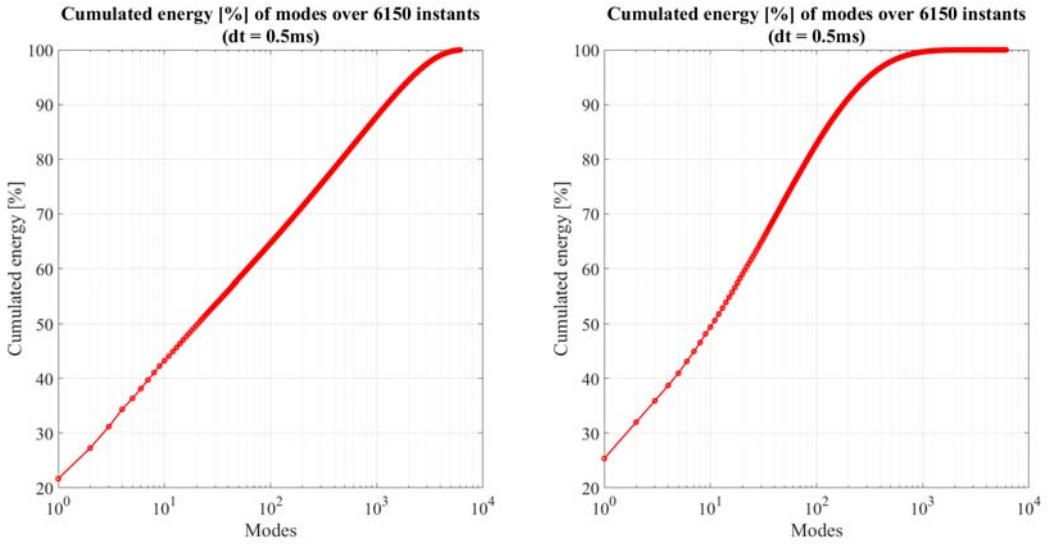

Figure 16: Cumulated energy as function of modes number – POD on PIV (on the left) – POD on LES (on the right)

The fluctuating energy contained in the first LES modes are slightly higher than PIV ones, but the global decreasing of energy is well captured. Since, at least 200 modes are required to get 90% of the total energy in LES (1000 modes in PIV), reconstruction of 2D velocity field via a

reduced order model (e.g. based on the 10 first modes) is not credible for the present industrial application (turbulent flow across a rod bundle). To illustrate this, the PSD on the right velocity probe have been reconstructed from POD modes on PIV measurement and LES results as function of the number of mode considered and compared to the original curves. The results are displayed on Figure 17 to Figure 19. For both PIV and LES, 500 modes allow a satisfactory reconstruction of the velocity PSD on the first 4/5th of the frequency range.

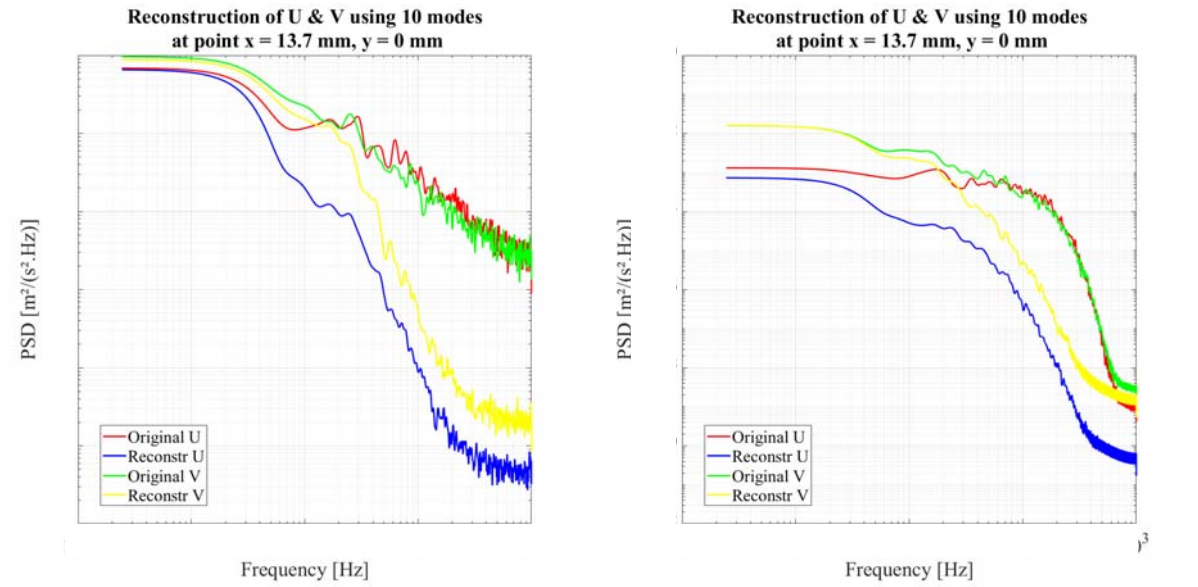

Figure 17: Reconstruction of PSD from POD on right probe as function of number of modes – PIV (on the left) – LES (on the right) – 10 modes

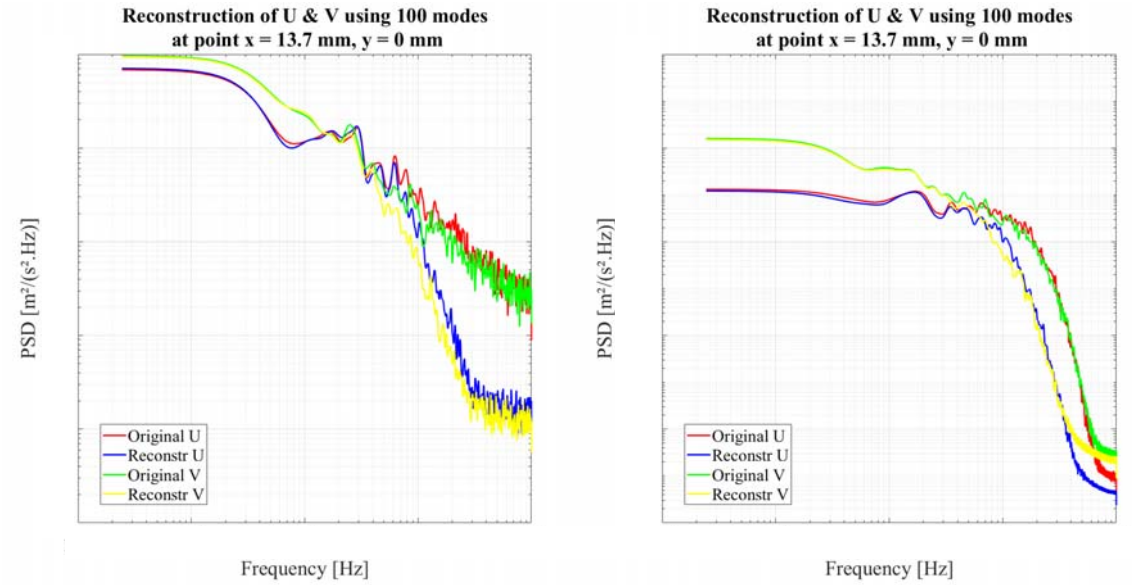

Figure 18: Reconstruction of PSD from POD on right probe as function of number of modes – PIV (on the left) – LES (on the right) –100 modes

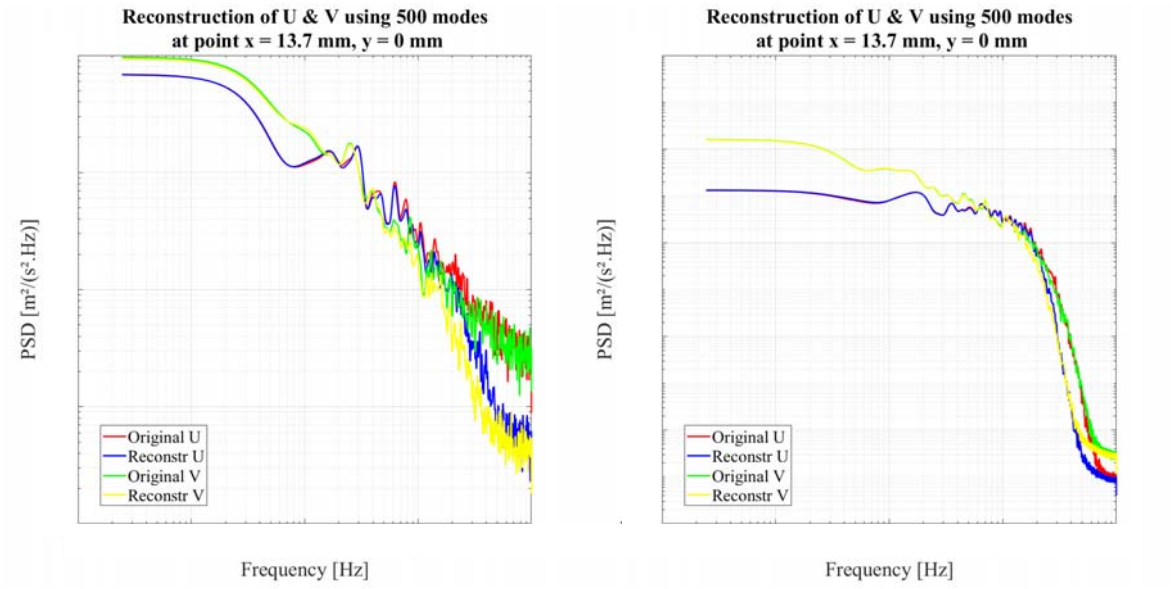

Figure 19: Reconstruction of PSD from POD on right probe as function of number of modes – PIV (on the left) – LES (on the right) – 500 modes

Secondly, the energy distribution among the 30 first modes is shown in Figure 20.

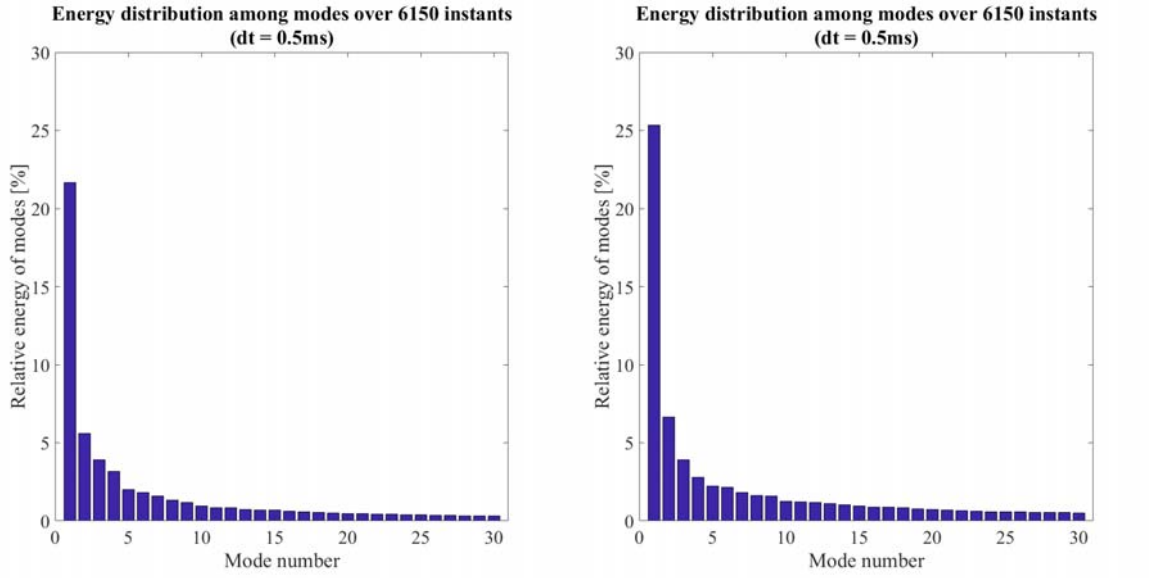

Figure 20: Energy distribution among modes – POD on PIV (on the left) – POD on LES (on the right)

The energy distribution for the 30 first modes appears similar between PIV and LES but the fluctuating energy content of PIV modes is 15% lower in accordance with the energy decrease described in Figure 16. The PIV distributes the fluctuating energy over a greater number of modes perhaps due to the experimental noise contained at high frequencies. The LES highest mode numbers contain indeed almost no fluctuating energy probably due to an over-dissipation of the sub-grid turbulent model. These modes could be indeed associated with the smallest turbulent scales and the highest fluctuating frequencies, in agreement with the PSD behaviour observed in Figure 14, Figure 15 and Figure 17 to Figure 19.

The spatial distributions $\vec{\phi}_k(\vec{x})$ of the 4 first modes (represented by streamlines) are compared between PIV and LES from Figure 21 to Figure 24.

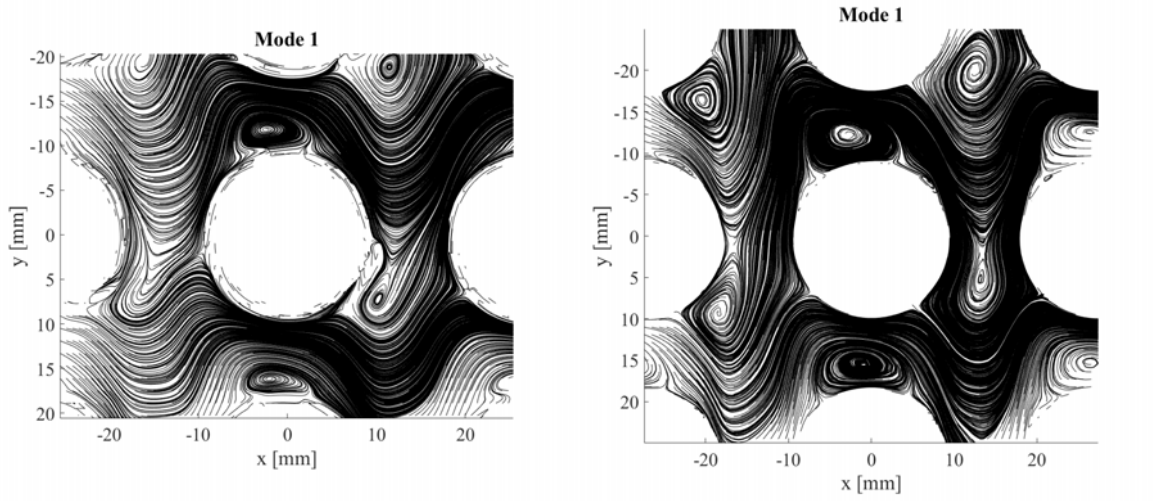

Figure 21: Spatial distribution of mode 1 – POD on PIV (on the left) – POD on LES (on the right)

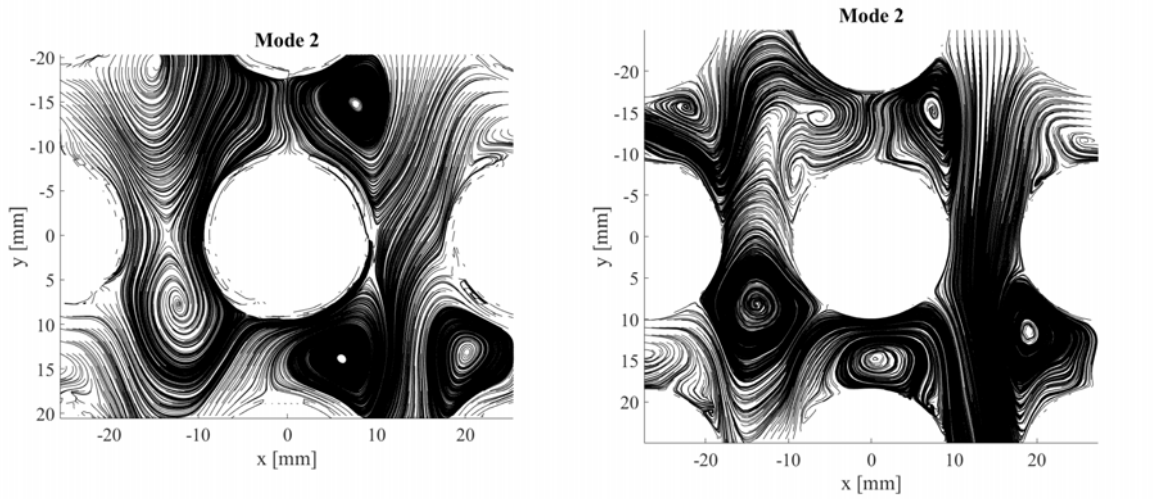

Figure 22: Spatial distribution of mode 2 – POD on PIV (on the left) – POD on LES (on the right)

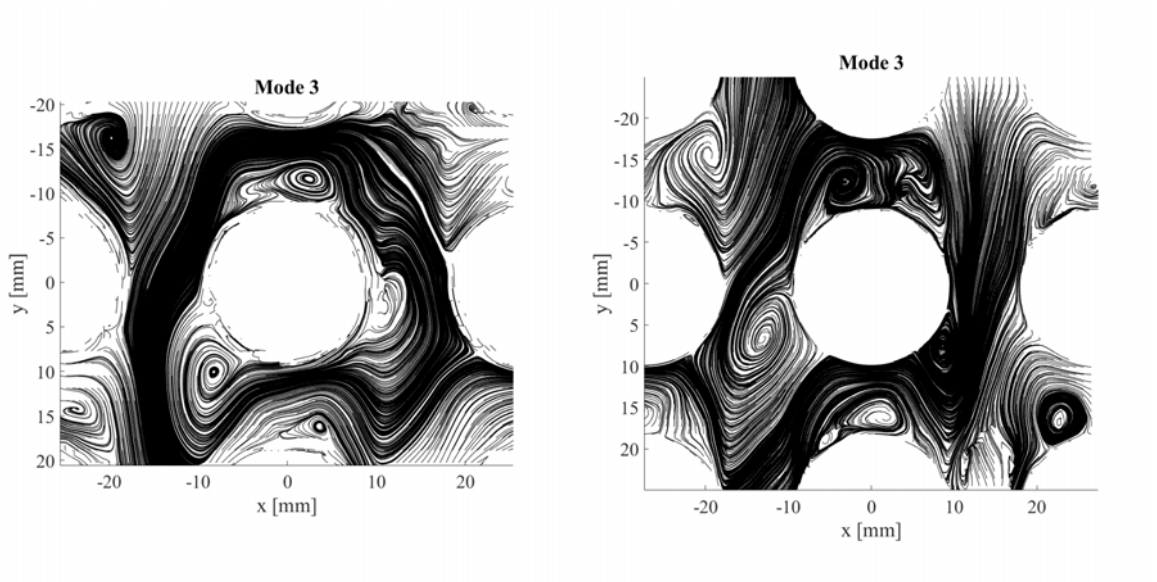

Figure 23: Spatial distribution of mode 3 – POD on PIV (on the left) – POD on LES (on the right)

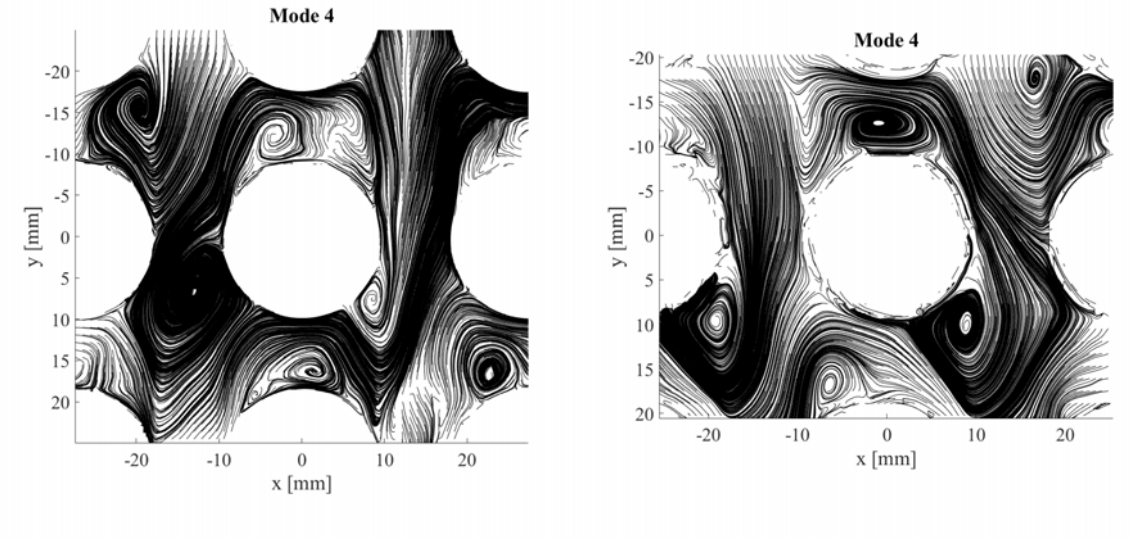

Figure 24: Spatial distribution of mode 4 – POD on PIV (on the left) – POD on LES (on the right)

The comparison of the mode spatial distributions underlines a good representation of the fluctuating energy flow behaviour by LES. After the 3rd mode, the spatial distribution are different meaning that a discrepancy should occur between LES and PIV leading to a different mode ranking of the one which has the 4th highest energy content. For instance, it is interesting to note the strong similarity between the 3rd mode of LES and the 4th mode of PIV. It would be interesting to examine further mode distributions to see if experimental mode distributions still exist at a further rank in the computation mode portfolio.

4.3.3. POD convergence on experimental measurements

Robustness of POD results has been checked on experimental side, using either 6150 time samples or 9999 time samples (maximum number of image pairs realizable with the hi-speed camera memory capacity).

The Figure 25 presents the relative energy distribution among the 30 first modes. The global decreasing shape of energy with increasing mode numbers is the same in both cases. The main difference concerns the relative weight of the first mode which is around 22% on POD with 6150 times samples and slightly over 25% on POD with 9999 time samples. The rise of the first mode, linked to lowest frequencies since a longer time signal increases its energy contribution, comes at the expense of the slight reduction of mode 3 and 4. The global shapes on the cumulative fluctuating energy (not shown in the present paper) are consequently quite similar in both cases.

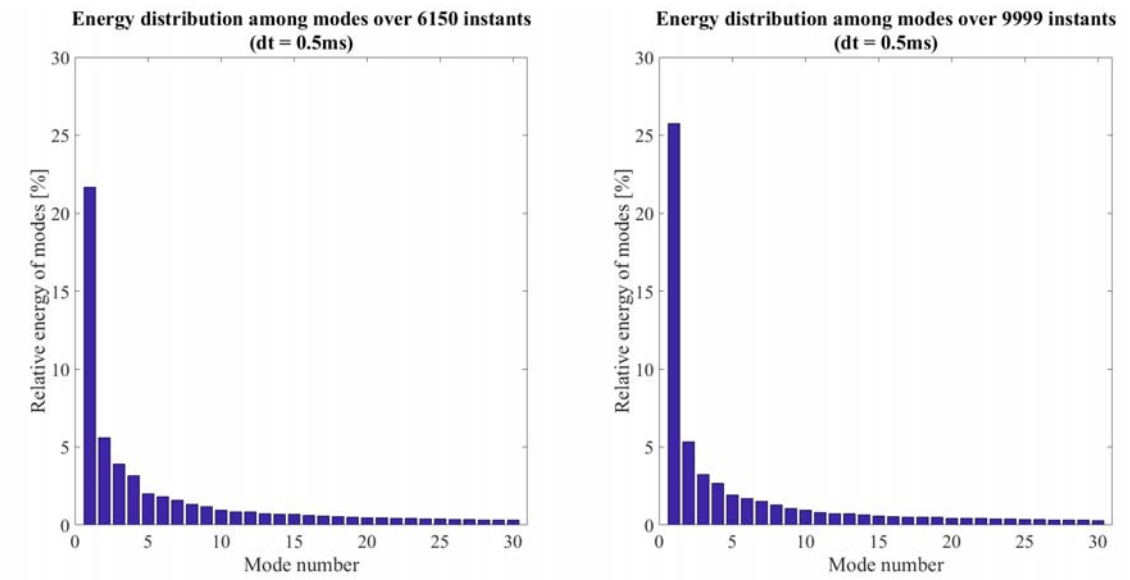

Figure 25: Energy distribution among modes – POD on 6150 PIV time samples (on the left) – POD on 9999 PIV time samples (on the right)

The 4 first modes spatial distribution $\vec{\phi}_k(\vec{x})$ represented with streamlines are displayed on Figure 26 to Figure 29. The location of vortices as well as their size is almost mixed-up on in both cases for the 4 first modes. For example, a slight difference is visible on the vortex on the left of the 6th tube (Figure 26 – red circles) for the 1st mode. Separation or convergence points are also invariant.

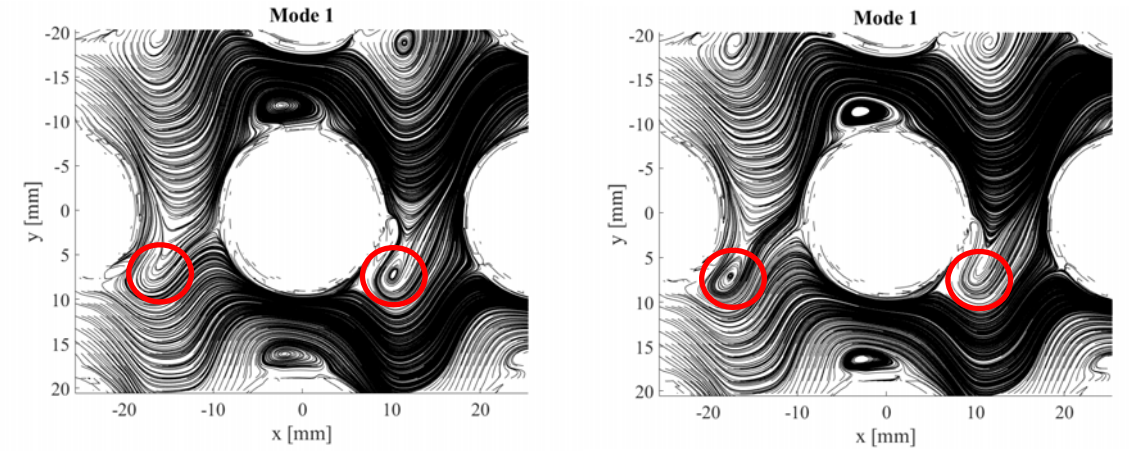

Figure 26: Spatial distribution of mode 1 – POD on 6150 PIV time samples (on the left) – POD on 9999 PIV time samples (on the right)

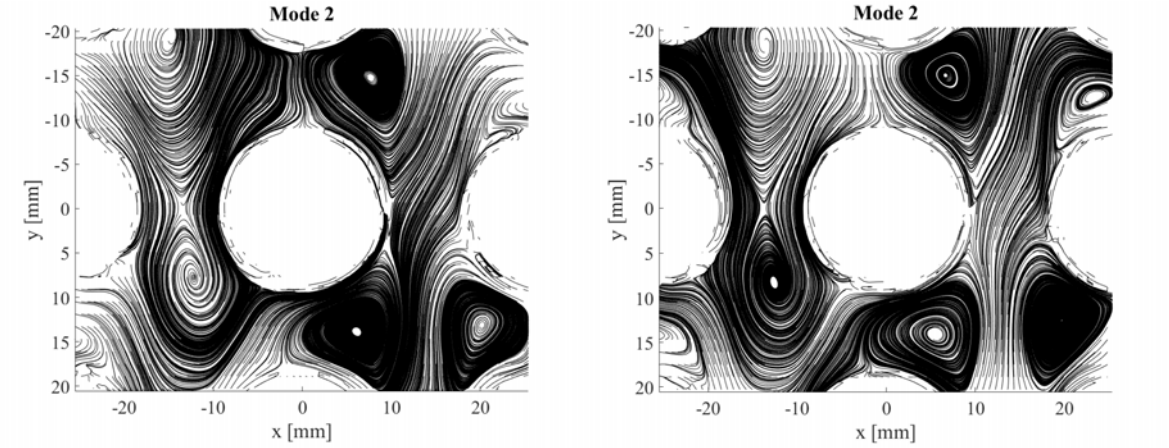

Figure 27: Spatial distribution of mode 2 – POD on 6150 PIV time samples (on the left) – POD on 9999 PIV time samples (on the right)

On the 3rd mode, the main change occurs on the vortex near the wall of the 6th tube on the right which is present on POD processing with 6150 time samples (red circle on Figure 28) and disappears on POD processing with 9999 time samples. The flow structure on the right of the 6th tube downstream shows also discrepancies.

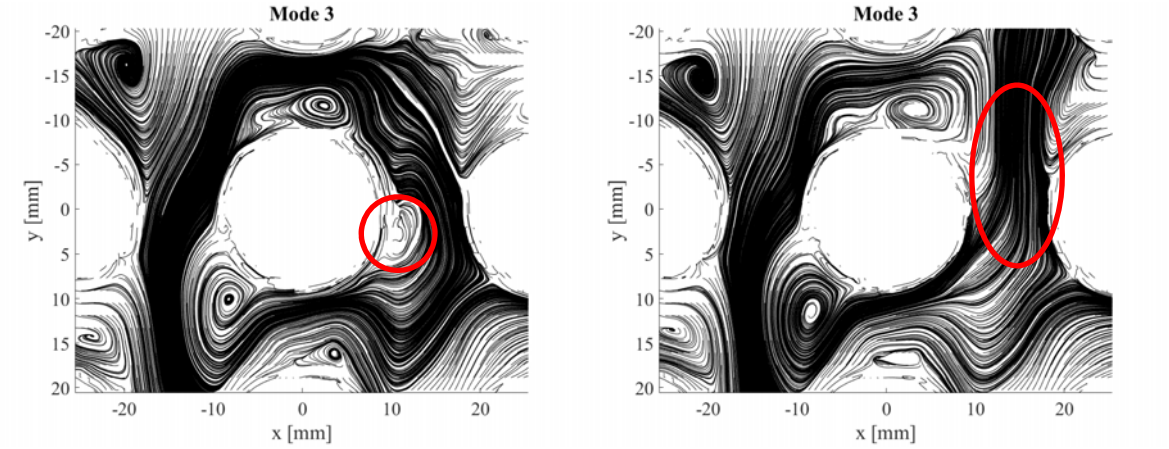

Figure 28: Spatial distribution of mode 3 – POD on 6150 PIV time samples (on the left) – POD on 9999 PIV time samples (on the right)

For the 4th mode, streamlines pictures are very similar.

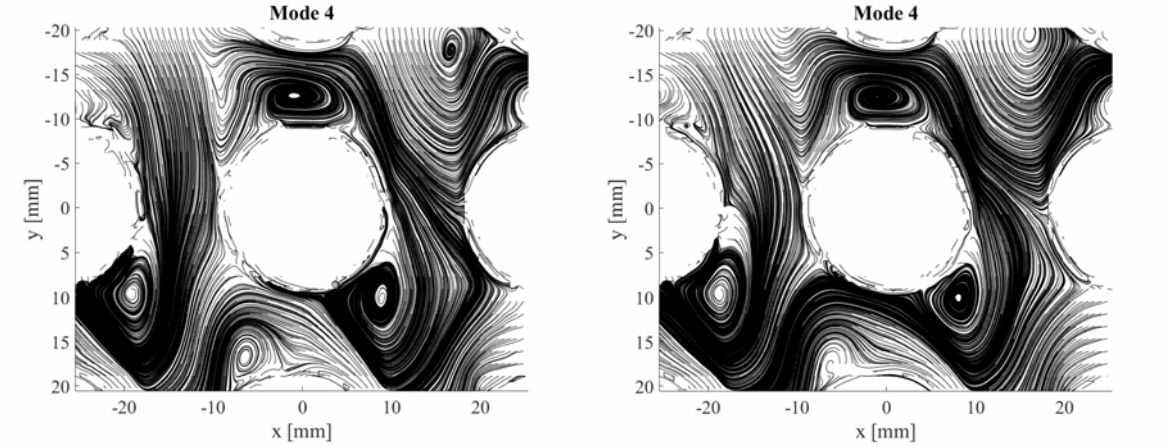

Figure 29: Spatial distribution of mode 4 – POD on 6150 PIV time samples (on the left) – POD on 9999 PIV time samples (on the right)

Regarding these results on POD processing using either 6150 time samples or 9999 time samples, it can be concluded that POD convergence, based on experimental pictures, is satisfactory. The same work will be performed on CFD results once 5 seconds of physical time simulation (same duration as PIV measurements) will be reached.

5. Conclusions

The purpose of this paper concerns the capability of the 3D CFD code FLUENT V15.0 to predict the single phase flow across a rod bundle using a Large Eddy Scale (LES) turbulence model. The ultimate goal of this work is to correlate turbulent fluctuation levels and frequencies to the excitation modes of the U-tubes (Fluid-Structure-Interaction) encountered for instance at the entrance of the tube bundle of Steam Generators (SG).

To give more insights into the turbulent flow across this configuration, a transparent rod bundle mock-up has been built. Non-intrusive velocity measurements have been realized to provide experimental data for CFD validation. Laser Doppler Velocimetry (LDV) and Particle Image velocimetry based cross-correlation (PIV) and based on Optical Flow (OF) computations have been carried out and compared to assess their reliability.

In parallel, a LES-Smagorinsky-Lilly turbulent model transient computation has been run for 3.1 seconds (same order of magnitude as PIV acquisition duration). During this simulation, velocity probes have been settled around the second last centred rod (6^{th} from upstream to downstream) in the mid-depth plane (zone of interest).

A standard spatial comparison of both time averaged (mean) and standard deviation velocity fields and profiles has demonstrated a good agreement between the CFD code predictions and the measurements. These elements enable AREVA NP to consider its computation scheme as validated on this application.

To go further in CFD validation, Power Spectral Densities (PSD) from LES are successfully confronted to all measuring techniques results at the left probe and to LDV spectra at all four probe locations. This validates the ability of the LES turbulent model to predict correctly the dynamical behaviour of the flow in the lower and medium frequencies.

Finally, POD analysis applied on PIV and LES compares the fluctuating energy distribution contained in the turbulent flow. POD convergence analysis, applied on the experimental fields, demonstrated that the flow structure obtained on the 4 first mode with 6150 time samples is quite similar with the one obtained with 9999 time samples. Although POD analysis does not allow generating a reduced order model able to reconstruct the turbulent flow with a limited number of modes for the present industrial application, this advanced comparison between PIV and LES results improves the confidence level of the validation of the code. Throughout the present study, the FLUENT software demonstrates the ability to predict correctly spatial, spectral and fluctuating energy (organisation into modes) distributions of the complex turbulent flow across a rod bundle.

Acknowledgments

The authors thank L. Zimmer (CNRS – EM2C laboratory - CentraleSupelec) for his support to the experimental work, especially on POD analysis and optical flow calculations.

Abbreviations

CFD: Computational Fluid Dynamics
DNS: Direct Numerical Simulation
LDV: Laser Doppler Velocimetry
LES: Large Eddy Simulation
OF: Optical Flow
PIV: Particles Image Velocimetry
POD: Proper Orthogonal Decomposition
PSD: Power Spectral Density
RANS: Reynolds Averaged Navier-Stokes
SG: Steam Generator
SL: Smagorinski-Lilly turbulent sub-model
URANS: Unsteady Reynolds Averaged Navier-Stokes

References

[1] Foreman, J. W.; George, E. W.; Lewis, R. D (1965), *Measurement of Localized Flow Velocities in Gases with a Laser Doppler Flowmeter*, Applied Physics Letters 7, pages 77-80.

[2] Veynante, D., Candel, S.M. (1988), *A promising approach in Laser Doppler Velocimetry: signal reconstruction and non-linear spectral analysis*, Signal processing 14, pages 295-300.

[3] Veynante, D., Candel, S.M. (1988), *Application of non-linear spectral analysis and signal reconstruction to Laser Doppler Velocimetry*, Experiments in Fluid 6, pages 534-540.

[4] Adrian, R.J. (1991), *Particle-imaging techniques for experimental fluid mechanics*. Annual Review of Fluid Mechanics. 23 (1), pages 261–304.

[5] Raffel, M.; Willert, C.; Wereley, S.; Kompenhans, J. (2007), *Particle Image Velocimetry: A Practical Guide*. Springer-Verlag. ISBN 3-540-72307-2.

[6] Adrian, R.J.; Westerweel, J. (2011), *Particle Image Velocimetry*. Cambridge University Press. ISBN 978-0-521-44008-0.

[7] Sun, D.; Roth, S.; Black, M. (2010), J. *Secrets of Optical Flow Estimation and Their Principles*, 23rd IEEE Conference on Computer Vision and Pattern Recognition (CVPR), pages 2432-2439.

[8] Jus Y. (2011), *Modélisation et simulation numérique de vibrations induites par écoulements autour d'obstacles cylindriques seuls ou en réseaux*. Ph. D, UPMC (13th december 2011).

[9] S. Aravind, K. Iver (2016) *Numerical Analysis over Transversely Oscillating Cylinder*, 6th International & 43rd National Conference on Fluid Mechanics and Fluid Power (FMFP-2016), Allahabad, Uttar Pradesh, India 2016.

[10] I. Afgan, (2007) *Large Eddy Simulation of Flow over Cylindrical Bodies using Unstructured Finite Volume Meshes*, Ph. D, University of Manchester.

[11] Lumley, J. L. (1981), *Coherent structures in turbulence.* In Transition and Turbulence, edition R. E. Meyer, pp. 215–241.

[12] Sirovich, L. (1987), *Turbulence and the dynamics of coherent structures, Parts I, II and III*. Quarterly of Applied Mathematics XLV, 561–590.